2D SINGLE-FOCUS FREQUENCY SCANNING ARRAYS FOCUSED IN THE FRESNEL ZONE

S. E. Bankov

Kotelnikov Institute of Radioengineering and Electronics of Russian Academy of Sciences, Mokhovaya11-7, Moscow125009, Russia

The paper is received on October 20, 2017

Abstract. 2D single-focus arrays of elementary radiators with frequency scanning focused in the Fresnel zone are considered. A problem of the array synthesis is solved for the arrays of different types. The proposed solution determines coordinates of the elementary radiators located in the planar aperture. An approximate analysis of the electromagnetic field radiated by the array of the radiators assuming specified currents is presented. The currents are formed by a system of parallel transmission lines loaded with the elementary radiators. Traces of focal spots movement in two dominant scanning planes - in parallel and perpendicular to the transmission lines axes - are investigated. Scanning curves determined for the field strength maximum and for the radiation efficiency maximum are obtained.

Key words: focused array, frequency scanning, Fresnel zone, scanning curve, radiation efficiency.

1. Problem formulation

At present near zone active and passive systems of microwave imaging are widely used for anti-terror inspection, detection of explosives, medicine diagnostic and in many other applications. A scanning or multi-beam radio-objective that forms images in the radio frequency range is the most important part of such systems. The theme of design and investigation of radio-objectives is presented in many articles [1–8].

The studied radio-objectives present antennas of different types which are focused in the Fresnel zone. These are antennas with mechanical scanning, phased arrays (PA), multi-beam reflector or lens antennas and others. The most interesting

for practical use are radio-objectives with electrical scanning capabilities enabling to form radio images in real time. Radio imaging systems usually operate at relatively high frequencies ranging from the upper part of centimeter band to terahertz band for providing high angular resolution. For the same purpose they need to have sufficiently large (relative to the operating wavelength) radiating aperture. PAs with such dimensions have large number of elements and therefore may have very high cost. Due to this factor, radio-objectives with hybrid scanning are often used. They monitor a certain area of space using mechanical scanning in one plane and electrical scanning in the orthogonal plane. The simplest way to realize hybrid scanning is to use a linear leaky-wave antenna [9]. Such objective can view the area along the antenna axis due to frequency variation, while the observations in the orthogonal plane can be performed mechanically [10,11]. Such hybrid scheme of scanning makes it possible to reduce the number of controlled elements and therefore the cost of the device without degradation of the resolution. Note that objectives of this type have no functionality and flexibility that are character for PAs.

Different types of linear leaky-wave antennas can be used for focusing its radiation field in the Fresnel zone. Among them are antennas on the base of a curved waveguide [14-15], straight-line waveguide with variable leaky-wave phase velocity [16, 17], straight-line waveguide loaded with an array of lumped radiators placed with variable period [18-20], helix [21] and radial line [22-23]. Note that the frequency scanning was studied only in [16, 17] in the case of linear leaky-wave array with a constant period of radiators.

2D arrays are more interesting than linear arrays due to their capability of forming focal spots while linear structures form focal curves. The field concentration in a focal spot is much higher than in a focal curve. A 2D frequency scanning array of low-directivity radiators focused at a distance of the order of the array aperture size is considered in [24], in which results of the study for a frequency scanning array of parallel rectangular slotted waveguides are presented. The radio-objectives using arrays of this type can view the space by combination of two types of scanning. In the plane parallel to the waveguides axes the frequency scanning is used. In the

orthogonal plane, scan of the focal spot can be achieved in different ways, for instance using phase shifters or beam-forming network (BFN). Such implementations are equivalent to formation of wave set exciting the waveguides of the focused array. We will denote those two planes as longitudinal and transversal planes respectively. It is possible to select dominant planes that cross antenna aperture center.

In [24, 25] it was shown that the frequency-scanning curve is non-symmetrical relative to the center point. Scanning curve of this type is not well suited for the radio-objective design. It was also found in [24, 25] that the waveguide focused arrays are characterized by appearance of side diffraction lobes even when dielectric-filled waveguides are used.

The goal of this work is investigation of 2D frequency scanning focused arrays from a more general point of view comparing with [24, 25]. In particularly the current study should determine the cause of the scanning curve asymmetry: weather it is fundamentally connected with the scanning method or only with a specific implementation of it.

To achieve the goal of the study we will develop a generalized model of the array. In many aspects it is similar to the model described in [24, 25]. The method of specified currents is used for the radiation field calculations. Each radiator presents an elementary source the field of which is defined in the scalar approximation. Amplitudes of sources are found in the single mode assumption assuming that only the dominant mode propagates in the transmission line (TL) loaded with radiators. The mode is described in terms of the generalized parameters, namely: propagation and attenuation constants γ and α. Unlike [24], here we do not fix the TL construction, but describe TL in the generalized form that suits for an arbitrary TL.

Using this approach, we can find the array radiation field and determine location of characteristic points: the maximum of the field strength and the maximum of energy efficiency. Their positions depend on the operating frequency in the longitudinal plane and on the array excitation circuit (AEC) operation regime in the transverse plane. Below we will study the scanning characteristics only in the main planes.

2. The structures under study and their synthesis

It should be noted that 2D focused arrays with frequency scanning can be constructed in a variety of ways. The general structure of the array is shown in Fig. 1. It contains a set of TLs each of which is loaded by a linear array of elementary radiators connecting with TL in series. The AEC is shown in the left part of Fig. 1. In general it has several input ports (in Fig. 1 one input port is shown) and M output ports. The number of output ports is equal to the number of TL.

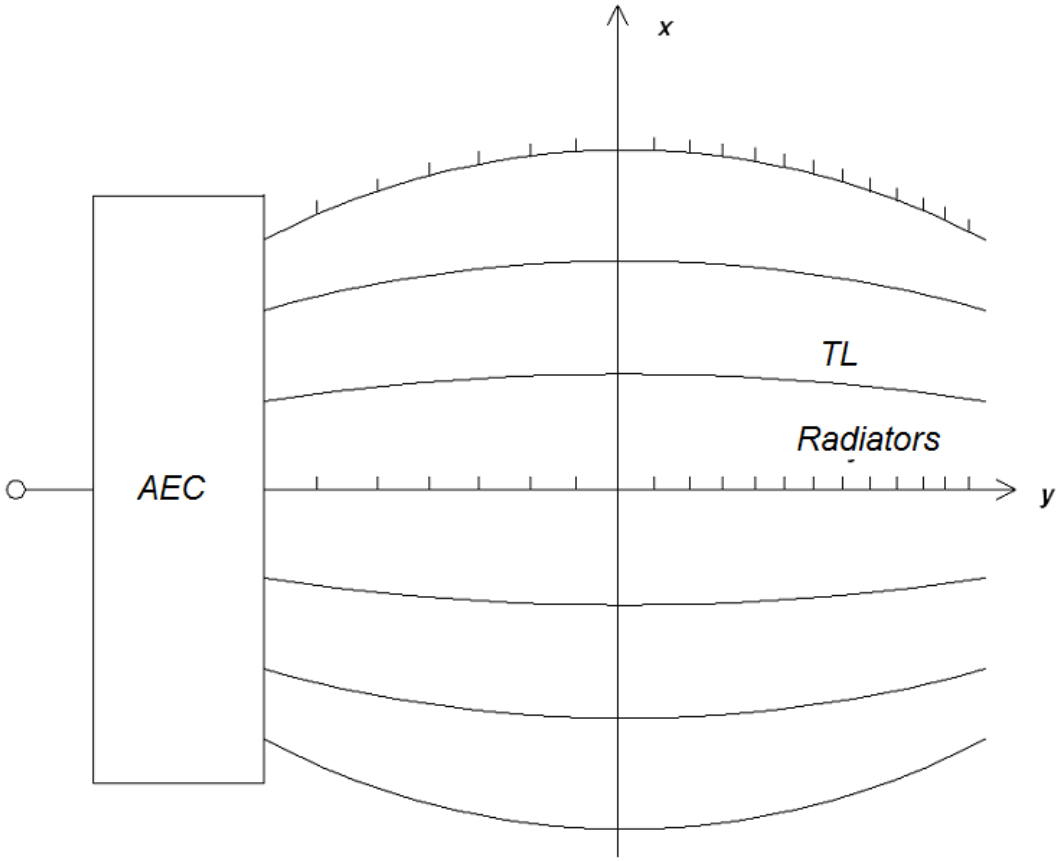

Fig. 1. General schematic structure of a focused array

In the general case the TL can have a curved shape and form a non-planar 3D structure not bounded by XOY plane. Here we will consider only planar arrays with straight-line TL (see Fig. 2).

A variety of focused arrays is determined by two factors: the array radiation regime and the AEC structure. Each TL with a set of radiators presents a leaky-wave linear array. It is known [26] that the electromagnetic field of a periodical antenna array may be expanded in the Floquet space harmonics series. A conventional array

has only one radiating space harmonic. Typically it is a zero order or minus first order harmonic. In the first case the wave slowing factor $U = \gamma / k < 1$, where k is the free space wave number. In the second case $U > 1$. Hence there are two different array operating modes: the regime of zero order radiating harmonic and the regime of minus first order radiating harmonic.

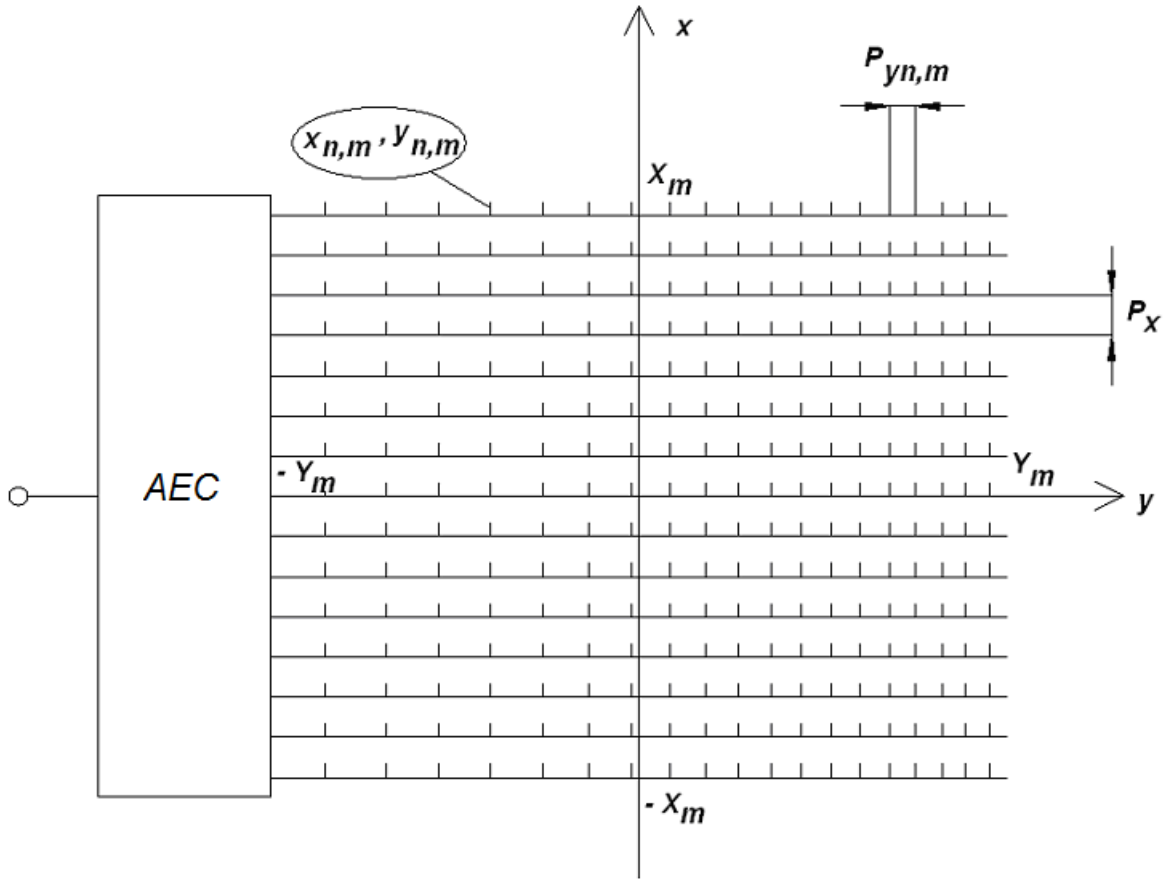

Fig. 2. Scheme of the considered array

The AEC can be designed in several ways. The maximum functionality is achieved by using a system of phase shifters inserted in TL. They provide an arbitrary phase distribution between the array channels. It is also possible to use a quasi-optical system, for example a Rothman lens [27] that produces a discrete number of phase distributions corresponding to the excitation of different lens inputs. Note that not all these distributions meet the conditions of perfect focusing due to the Rothman lens aberrations.

Zoned lens combined with a multi-channel power divider can be also applied as an AEC. It is the simplest technical solution for scanning in the longitudinal plane.

Below both modes of the array radiation will be considered. For the arrays with minus first radiating harmonic two subtypes will be selected: the array with a constant period and the array with a constant slowing factor. The meaning of this subdivision is explained below when considering the array synthesis problem. Here we will use the structure with a set of phase shifters as a basic type of AEC. We will also briefly discuss the influence of a zoned lens on the scanning in the longitudinal plane.

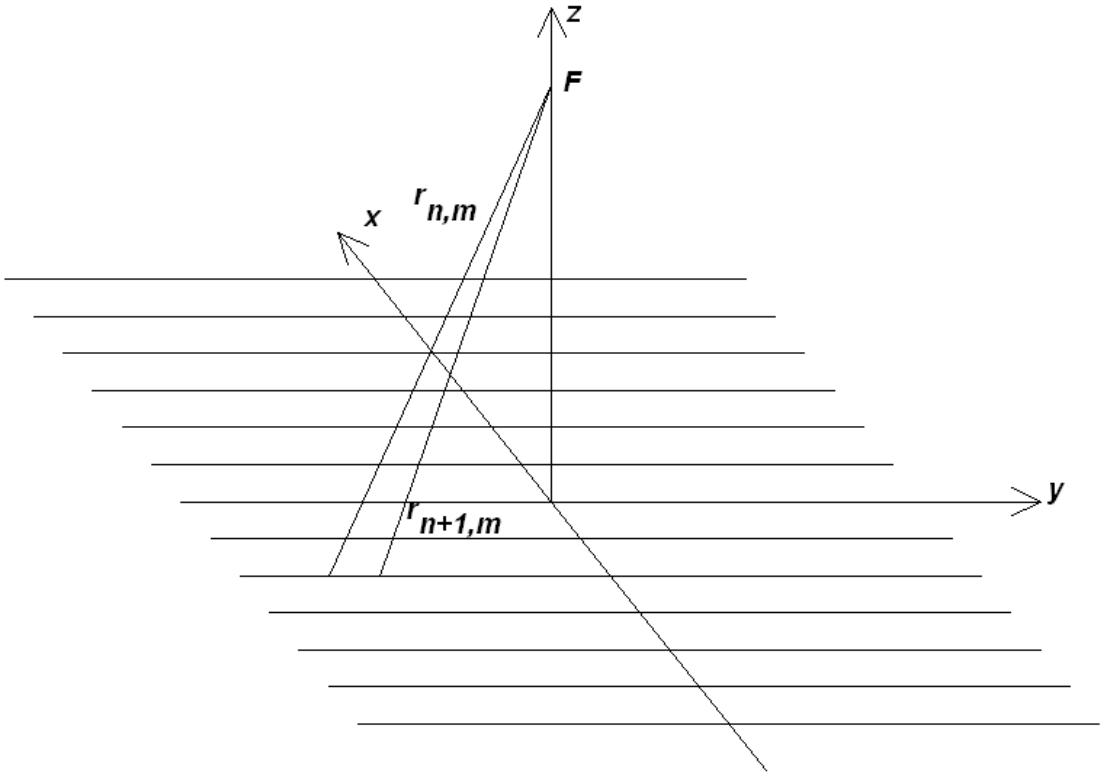

Fig. 3. To the illustration of the array synthesis method

The synthesis procedure is explained in Fig. 3. We perform it in two stages. At the first stage, the in-phase condition is used for all beams coming to the focal point F from all the radiators in TL with an arbitrary number m. This condition has the following form:

$$U_{n,m}P_{yn,m} + r_{n+1,m} - r_{n,m} = -\frac{2\pi\nu}{k_0}, \qquad (1)$$

$$P_{yn,m} = y_{n+1,m} - y_{n,m},$$

$$r_{n,m} = \sqrt{x_m^2 + (y_{n,m} - y_f)^2 + F^2},$$

$$x_m = mP_x,$$

where $U_{n,m}$ is the slowing factor of the m-th TL in the interval $y_{n,m} < y < y_{n+1,m}$, k_0 is the free space wave number at the frequency of synthesis f_0, ν is a number of the array space harmonic, P_x is the period of the TL array (the distance between adjacent TL).

Equation (1) is written for the focal point with coordinates $(0, y_f, F)$ and the time dependence is assumed to be $\exp(i\omega t)$. It is reduced to a biquadratic equation for the value $y_{n+1,m}$ that has the solution in the following form:

$$y_{n+1,m} = \psi(y_{n,m}, U_{n,m}), \qquad (2)$$

where ψ is a known function. Expression (2) makes it possible to build an iterative procedure that expresses $y_{n,m}$ via the arbitrary specified coordinate of the leftmost radiator $y_{0,m}$. In so doing we have the free parameter $y_{0,m}$. Also there is an additional degree of freedom due to a free choice of the slowing factors $U_{n,m}$. So we can obtain an infinite number of the synthesis problem solutions. In this work we consider two of them: the array with a constant slowing factor $U_{n,m} = U$ and the array with a constant period $P_{yn,m} = P_y$. Note that in [24] the array variant with a constant slowing factor was studied.

At the second stage of the synthesis, in-phase summation at the focal point of all beams with $n = 0$ need to be provided. As noted above, this condition can be satisfied by different ways. Let the leftmost radiator is located at the left edge of the array aperture $y_{0,m} = -Y_m$ (see Fig. 2). Then the in-phase condition has the following form:

$$\varphi_m - k_0 r_{0,m} = C + 2\pi q_m, \qquad (3)$$

where φ_m are phases of the waves formed by AEC, C is an arbitrary constant that may be for example equal to $\varphi_0 - k_0 r_{0,0}$. When $q_m \neq 0$ condition (3) provides in-phase summation of the beams with an accuracy of 2π.

Assuming an optical system used as an AEC, condition (3) can be satisfied for $q_m = 0$. In this case the optical system will concentrate field at a point located at the distance $\sqrt{F^2 + (Y_m + y_f)^2}$ from it. Note that for an optical system condition (3) will be satisfied not only at frequency f_0, but at any frequency f.

The phase shifters provide phase shifts in the interval from zero to 2π. It means that $q_m \neq 0$ in equation (3). Jumps by 2π in phase values are usually considered as a source of errors in the phase distribution destroying it in the frequency range. However, assuming that the phase shift is frequency dependent then no errors occur and equation (3) can be satisfied for any k. In this case the system of phase shifters is equivalent to an optical system.

If $y_{0,m} \neq -Y_m$ then the following solution of equation (3) exists:

$$-k_0 U (y_{0,m} + Y_m) - k_0 r_{0,m} = C + 2\pi q_m . \qquad (4)$$

It is written for $\varphi_m = const$ which corresponds to the array excitation by an in-phase power divider. Relation (4) is an equation in coordinates $y_{0,m}$. The TL sections from the leftmost edge point to the points $y = y_{0,m}$ act as a zoned lens.

Equation (1) has solutions when the focal point coordinate y_f changes in a wide range in the radiation mode at minus 1 space harmonic. Consider next the most interesting arrays focused in the point located over the aperture center, in which case $y_f = 0$.

It is impossible to focus radiation over the array in the zero-order operating mode. It follows from equation (1) and has a clear physical explanation. The zero-order space harmonic radiation is possible only for TL with fast wave $U < 1$. The angle of radiation of each array section is determined from the following relation:

$$\theta = \arcsin\frac{U}{k}. \qquad (5)$$

The angle θ is measured between the direction of radiation and the normal to the array plane. Formula (5) is written for the wave propagating from left to right. From (5) it is clear that $\theta > 0$. It means that all array points radiate in the direction of the wave propagation while focusing in the point over the array plane requires the backward radiation in some points. Therefore the following inequality should be satisfied for the array in the zero-order radiating mode:

$$y_f > Y_m.$$

Let a hollow rectangular waveguide is used as a TL with a fast wave. In this case we have for $U_{n,m}$:

$$U_{n,m} = \sqrt{1-\left(\frac{\pi}{ka_{n,m}}\right)^2}, \qquad (6)$$

where a is the size of the wide waveguide wall. From (1) obtain the following solution for $a_{n,m}$:

$$a_{n,m} = \frac{\pi}{k_0\sqrt{1-\left(\frac{r_{n,m}-r_{n+1,m}}{P_{yn,m}}\right)}}. \qquad (7)$$

Coordinates $y_{n,m}$ in (7) can be specified in an arbitrary way. Assume that the radiators are placed periodically: $P_{yn,m} = P_y$. The waveguide width varies in the limited range:

$$\pi < ka < 2\pi. \qquad (8)$$

Inequality (8) ensures the propagation of the dominant waveguide mode and absence of propagating higher order modes. It must be valid for all $a_{n,m}$ and it limits the frequency scanning range.

It is also reasonable to impose the condition of side diffraction lobes suppression. This condition is rigorously formulated for periodic arrays. For the considered non-periodic structures this condition can be formulated only locally.

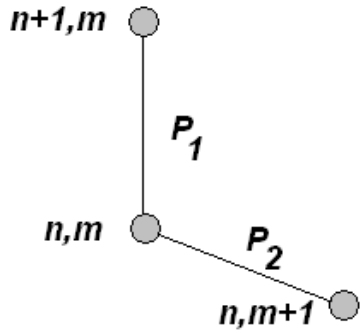

Fig. 4. Group of elements in non-periodical array

Select one array element that is characterized by indexes n,m and adjacent radiators with $n+1,m$ и $n,m+1$ as shown in Fig. 4. This group of elements can be considered as an element of a periodical array with a skewed lattice and periods $P_{1,2}$. As the phase shifts between the radiators are known it is possible to write down the condition of side lobes absence for the equivalent periodical array. However it is more convenient to use the stricter condition that provides the required side lobes suppression irrespective on the value of the phase shifts:

$$P_x, P_{yn,m} < \lambda / 2, \qquad (9)$$

where λ is a free space wavelength. Inequality (9) must be satisfied at all operating frequencies.

For periods satisfying the relation (9) the array periodicity does not significantly affects the characteristics of its radiation. Due to this, it becomes possible to replace the set of point sources by their continuous distribution in the antenna aperture. Such distributions are convenient for an analytical study of the array characteristics. The continuous phase distributions $\varphi(x', y')$ for different types of arrays are given below without their derivation:

$$\varphi = \begin{cases} -(k-k_0)U(y'+Y_m) + k_0\sqrt{x'^2+y'^2+F^2} + (k-k_0)\sqrt{x'^2+Y_m^2+F^2}, \\ -\dfrac{2\pi}{P_y k_0}(k-k_0)(y'+Y_m) + k\sqrt{x'^2+y'^2+F^2}, \\ -k_0 \int\limits_{-Y_m}^{y'} \sqrt{\dfrac{k^2}{k_0^2} - \dfrac{x'^2+F^2}{x'^2+(y-y_f)^2+F^2}}\,dy + k\sqrt{x'^2+(Y_m+y_f)^2+F^2}, \\ -\dfrac{2\pi}{P_y k_0}(k-k_0)(y'+Y_m) + k\sqrt{x'^2+y'^2+F^2} + Q(x'), \end{cases} \quad (10)$$

$$Q(x') = kUL(x'),$$

$$L(x') = \frac{1}{U}\left(\sqrt{x'^2+Y_m^2+F^2} - \sqrt{Y_m^2+F^2} - 2\pi\left[\frac{\sqrt{x'^2+Y_m^2+F^2} - \sqrt{Y_m^2+F^2}}{2\pi}\right]\right),$$

where the square brackets mean the operation of taking the integer part.

The first line in (10) corresponds to the array operating at minus first space harmonic with a constant slowing factor, the second line corresponds to the constant period array operating at minus first harmonic, the third line corresponds to the array operating at zero harmonic and the fourth line corresponds to the zoned lens array operating at minus first harmonic. The remaining structures have their AEC in the form of an ideal optical system or a phase shifter system. All arrays except the array operating at the zero harmonic mode have $y_f = 0$.

Nonessential terms that do not depend on coordinates are omitted in the phase distributions (10). One can see that at frequency f_0 all the distributions provide perfect focusing since adding to them phase shifts from any point in the aperture to the focal point gives a function that does not depend on the source coordinates x', y'.

3. Analytical study of arrays operating at the minus first harmonic in the paraxial approximation

In this section we consider the characteristics of long-focus arrays in the so called paraxial approximation. It is valid if the following relations are satisfied:

$$F^2 >> x'^2 + y'^2,$$

$$z^2 >> x'^2 + y'^2, \quad (11)$$

$$z^2 >> x^2 + y^2,$$

where x, y, z are coordinates of the point of observation.

Relations (11) allow us to expend the square roots in Eq. (10) in inverse powers of *F* and keep only the first two of them. Neglecting inessential constants we obtain the following approximate expressions for the phase distributions of the fields in the array:

$$\varphi = \begin{cases} -(k-k_0)Uy' + k\dfrac{x'^2}{2F} + k_0\dfrac{y'^2}{2F}, \\ -\dfrac{2\pi}{P_y k_0}(k-k_0)y' + k\dfrac{x'^2+y'^2}{2F}. \end{cases} \quad (12)$$

Two lines in (12) correspond to the arrays operating at the minus first harmonic with a constant slowing factor and a constant period. Then let us make similar transformations for the phase shift φ_r from the point $(x', y', 0)$ in the aperture to the observation point $(0, y, z)$:

$$\varphi_r = -kz - k\frac{y^2}{2z} + k\frac{yy'}{z} - k\frac{x'^2+y'^2}{2z}. \quad (13)$$

Expression (13) is given for $x = 0$, which corresponds to the main longitudinal scanning plane. Omitting the terms that do not depend on the coordinates x', y' obtain the total phase shift $\psi = \varphi + \varphi_r$:

$$\psi = \begin{cases} -(k-k_0)Uy' + k\dfrac{x'^2}{2F} + k_0\dfrac{y'^2}{2F} + k\dfrac{yy'}{z} - k\dfrac{x'^2+y'^2}{2z}, \\ -\dfrac{2\pi}{P_y k_0}(k-k_0)y' + k\dfrac{x'^2+y'^2}{2F} + k\dfrac{yy'}{z} - k\dfrac{x'^2+y'^2}{2z}. \end{cases} \quad (14)$$

We choose the coordinate y of the observation point so that the terms linear in y' vanish:

$$y = \begin{cases} \dfrac{(k-k_0)U}{k}z, \\ \dfrac{2\pi}{P_y k_0}\dfrac{(k-k_0)}{k}z. \end{cases} \quad (15)$$

To minimize phase variations, the parameter z should be chosen from the condition that the quadratic in y' terms vanish. However for a system with a constant slowing factor this cannot be done since the phase distribution has different quadratic terms in different coordinates x' and y'. In other words phase distortions-aberrations take place already at the level of quadratic terms.

For an array with a constant period the aberrations of this type are absent. Therefore, assuming $z = F$ we ensure that the quadratic part of the phase distribution is equal to zero. For an array with a constant slowing factor, we choose the distance z so that the quadratic terms vanish on average. As a result, we obtain the following relations:

$$z = \begin{cases} \dfrac{2kF}{k + k_0}. \\ F. \end{cases} \qquad (16)$$

Eliminating the parameter k from formulas (15), (16), we obtain the equations for the scanning curves of arrays:

$$z(y) = \begin{cases} F + \dfrac{y}{2U}, \\ F. \end{cases} \qquad (17)$$

It is seen from (17) that even in the paraxial approximation both arrays demonstrate different behavior. The array with a constant slowing factor cannot be perfectly focused in the frequency range, and its scanning curve has a form asymmetrical with respect to the origin. On the contrary, the array with a constant period can be focused to within quadratic phase terms and has a symmetric curve of scanning.

The obtained result gives an answer to the question formulated in Sec. 1 concerning the asymmetric scanning curve of the array investigated in [24]. It belongs to the type of arrays with a constant slowing factor and, as follows from formula (17), has an asymmetric scanning curve. In addition, it is seen from (17) that the asymmetry is stronger the smaller is the slowing factor U. Since the structure based on a waveguide with a low slowing ($U < 1$) was considered in [24], asymmetry

manifests itself very strongly in it. Thus we come to the conclusion that the discussed effect is related to the specific type of TL, and not to the principle of scanning.

4. Numerical study of focused arrays scanning in the main longitudinal plane

To calculate the intensity of the array field $V(x,y,z)$ we use the well-known formula [28]:

$$V(x,y,z)=\frac{1}{4\pi}\sum_{n=1}^{N}\sum_{m=1}^{M}A_{n,m}\frac{\exp(-ikr_{n,m})}{r_{n,m}}, \quad (18)$$

$$r_{n,m}=\sqrt{(x-x'_m)^2+(y-y'_{n,m})^2+z^2},$$

$$A_{n,m}=a_{n,m}\exp(i\varphi(x'_m,y'_{n,m})),$$

where $\varphi(x,y)$ is the phase distribution of sources and $a(x,y)$ is their amplitude distribution. As noted above, in the framework of the adopted model the field in the TL is represented by the field of the dominant mode traveling from the left to the right. In this case the following expression for $a_{n,m}$ takes place:

$$a_{n,m}=C\exp(-n\Delta), \quad (19)$$

where Δ is the wave attenuation per each radiator, C is a normalized multiplier. It is selected from the condition that the power of losses in the TL is equal to the power radiated into the free space in accordance with the method described in [24].

The most interesting for us is the position of the maximum of the function $V(x,y,z)$ that determines the scanning curve. We will also calculate and investigate a parameter equivalent to the coefficient of surface efficiency (CSE) which is widely used in the antenna theory:

$$K=\frac{\left|\sum_{n,m}A_{n,m}\frac{\exp(-ikr_{n,m})}{r_{n,m}}\right|^2}{\sum_{n,m}\left|A_{n,m}\right|^2\sum_{n,m}\frac{1}{r_{n,m}^2}}. \quad (20)$$

The parameter K shows how much of the power radiated by a lumped source located in the point (x,y,z) is received by the array with the specified field distribution in its aperture. We will also determine the scanning curve by the criterion

of CSE maximum.

Consider first the arrays radiating at the minus first space harmonic. Fig. 5 – 7 a, b show the scanning curves $z_s(y_s)$ (Fig. 5 – 7 a) and the dependencies of the normalized maximum value of the field intensity on the coordinate y_s located on the scanning curve (Fig. 5 – 7 b). The normalization is carried on the value of the intensity at the synthesis frequency f_0. Curves 1 – 3 are obtained for different types of arrays. Curve 1 corresponds to an array with a constant slowing factor and a system of phase shifters, curve 2 refers to an array with a constant period and a system of phase shifters and curve 3 to an array with a constant period and a zoned lens. In arrays with a constant period, the period P_y is determined from the following condition:

$$P_y = \frac{2\pi}{k_0 U}, \qquad (21)$$

where U is the corresponding parameter in the array, in which this parameter remains constant. Equality (21) provides the conditions for the correct comparison of arrays of different types.

The curves in Fig. 5 a, b are obtained for $F = 1000$, $U = 2$, $X_m = Y_m = 300$, $f_0 = 10$ ГГц, $\Delta = 0$. The frequency varies from 8.5 to 12 GHz. All dimensions here and hereafter are given in millimeters. From Fig. 5 a it is seen that the scanning curve does not pass through the predicted focal point. It is located below it. An array operating at the minus first harmonic and with a system of phase shifters has the most symmetrical scanning curve. Scanning curves of the other arrays are asymmetric. The strongest asymmetry takes place for an array with a constant slowing factor.

The dependence of the maximum field intensity V_m on coordinate y_s allows us to evaluate the range properties of the array, since the coordinate value is uniquely related to the frequency. The dependence of the parameter y_s on frequency is shown in Fig. 8. The curve is obtained for the parameters given above and the array with a constant slowing factor. Curves for other arrays are not given, since they differ slightly.

The array with a constant period and a system of phase shifters has the widest bandwidth (curve 2 in Fig. 5 b). The array with a constant slowing factor is worse at low frequencies and the array with a zoned lens is worse at high frequencies. Such situation is observed in all the numerical examples considered in this work.

Note that curves 1 – 3 in Fig. 5 a, b intersect at one point, which corresponds to the synthesis frequency f_0. At this frequency, all the structures have the same source distributions in the aperture and consequently the same position of the maximum points and the same field intensity values.

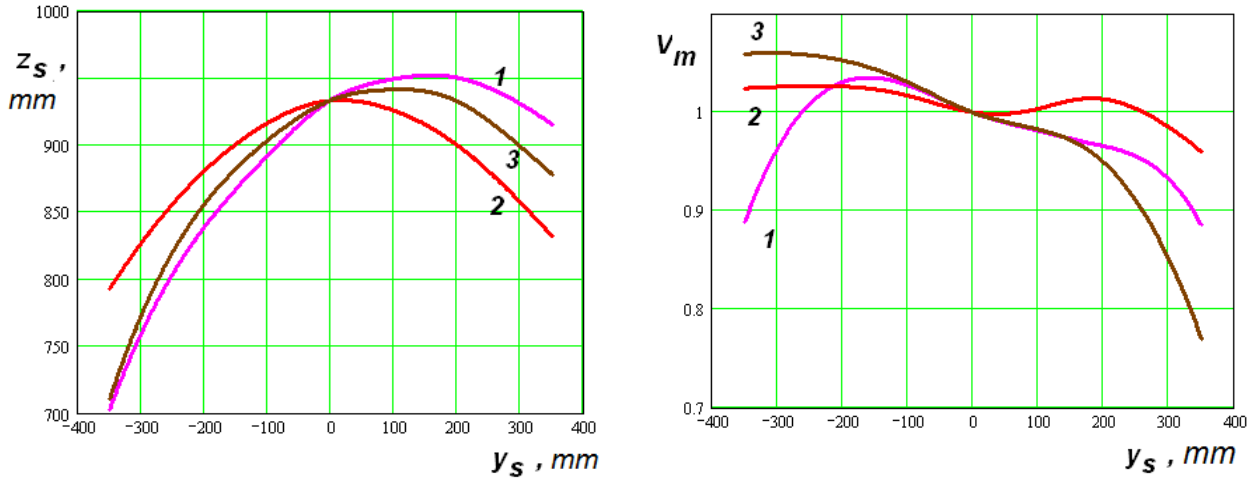

a b

Fig. 5. Parameters of scanning of arrays in the minus first operating mode with $F = 1000$. Maximum intensity definition.

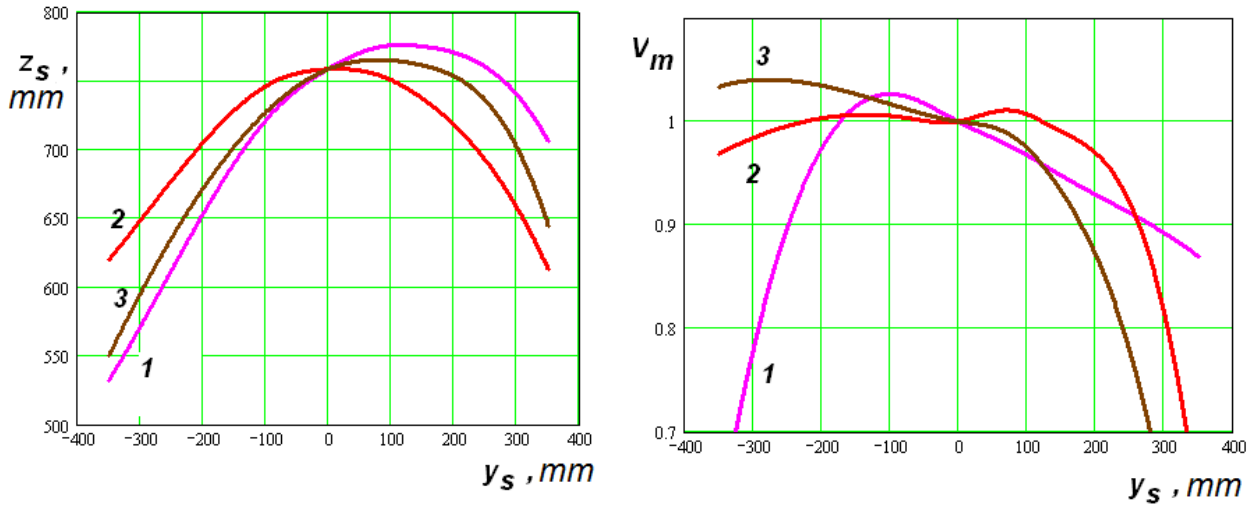

a b

Fig. 6. Parameters of scanning of arrays in the minus first operating mode with $F = 800$. Maximum intensity definition.

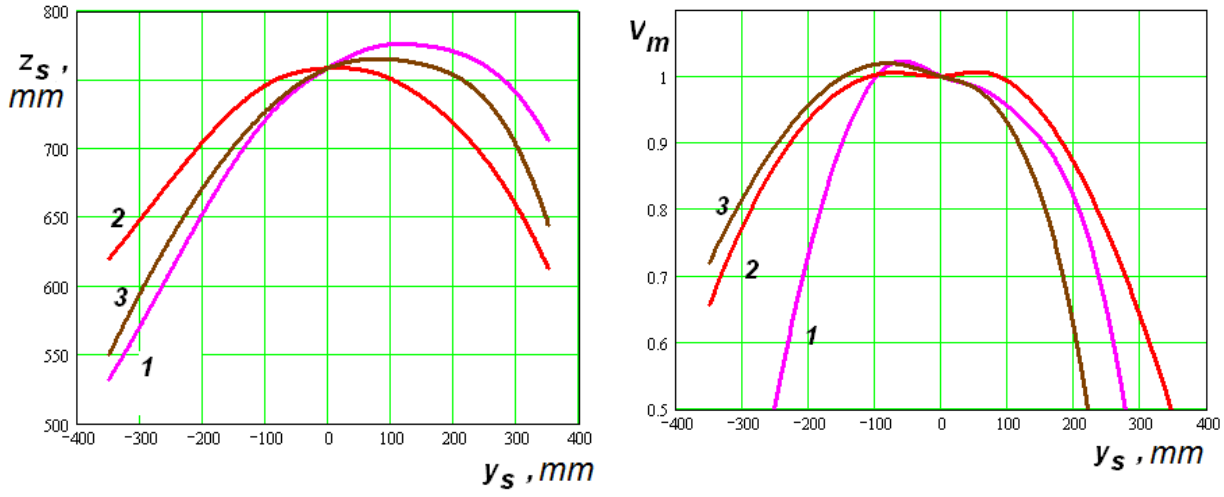

a b

Fig. 7. Scan parameters for arrays operating at minus first harmonic with $F = 600$. Maximum intensity definition.

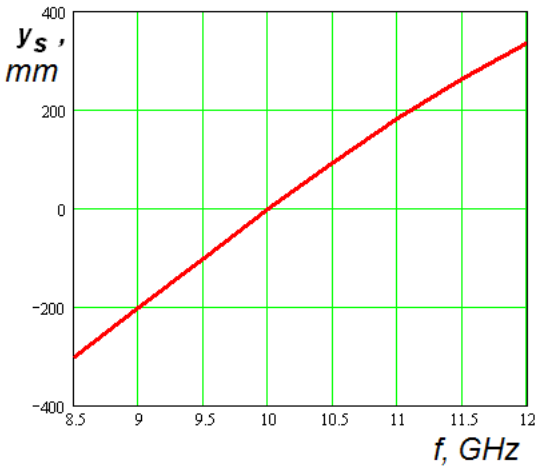

Fig. 8. Coordinate y_s vs. frequency

The scanning curves and the distributions of the maximum field intensity along them are presented in Fig. 6,7 a, b. Curves 1 – 3 are obtained for the parameters given above except for the focal distance F, which is 800 for Fig. 6 a, b and is 600 for Fig. 7 a, b. It can be seen that decrease of the focal distance leads to increase in the displacement of the maximum intensity point along $0z$ axis for all the arrays. It is also possible to note the narrowing of the bandwidth and correspondingly the area of scanning along the $0y$ axis. This narrowing is due to decrease in the field intensity at the boundaries of the frequency range. It could be expected since the level of aberrations in short-focus optical systems is always higher than in long-focus ones.

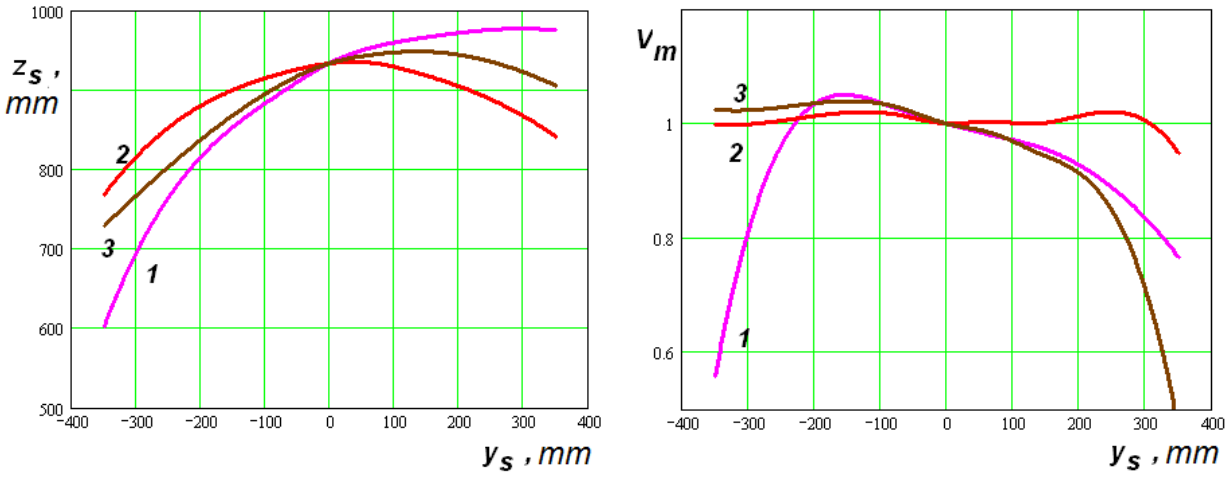

a b

Fig. 9. Scan parameters for arrays operating at minus first harmonic with $U = 1.5$. Maximum intensity definition.

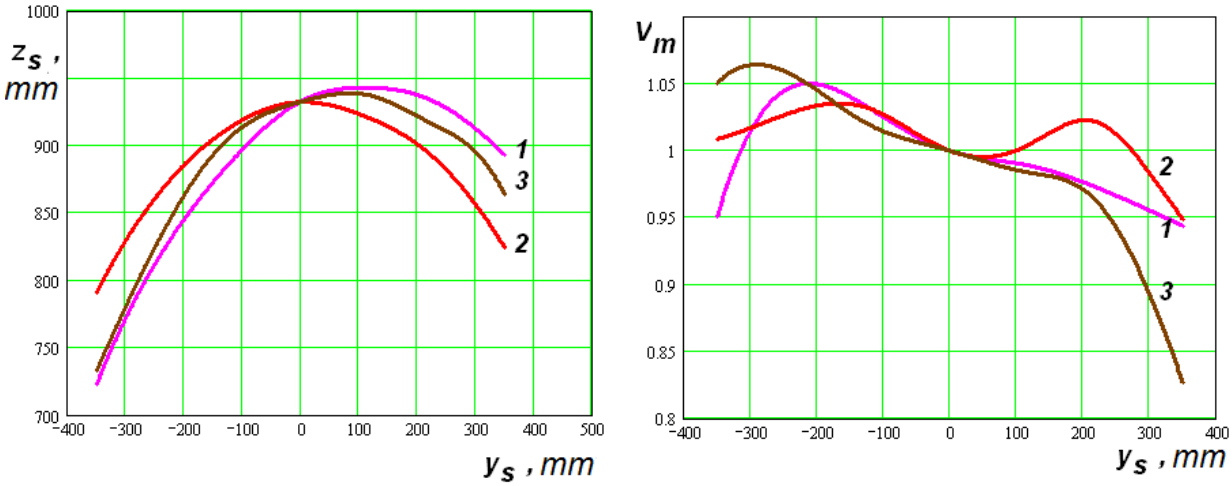

a b

Fig. 10. Scan parameters for arrays operating at minus first harmonic with $U = 2.5$. Maximum intensity definition.

The scanning curves and the distributions of the maximum field intensity along them are shown in Fig. 9, 10 a, b. Curves 1 – 3 are obtained for the parameters given above except for the parameter U, which is U =1.5 and U =2.5 for Fig. 9 a, b and Fig. 10 a, b, respectively. The focal distance F= 1000. Note that decrease of the slowing factor increases the difference between the scanning curves of different types of arrays. Thus, the asymmetry of the scanning curve of an array with a constant slowing factor is much greater for $U = 1.5$ then for $U = 2.5$. This result corresponds to the conclusions of the analytical study given in Sec. 3.

Increase in the slowing factor improves the scanning characteristics of all the arrays under considered (see Fig. 10 a, b). The decrease in the field intensity at the edges of the scanning sector decreases (Fig. 10 b) and scanning curves approach each other (Fig. 10 a).

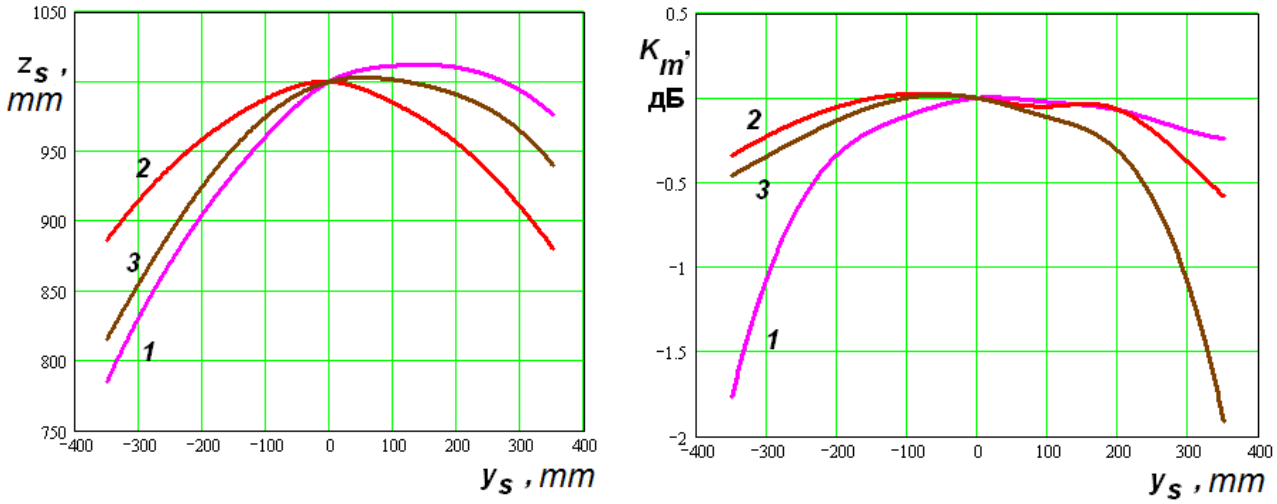

a b

Fig. 11. Scan parameters for arrays operating at minus first harmonic. Maximum CSE definition.

Let us further investigate the behavior of the scanning parameters determined with help of CSE (formula (20)). Looking ahead, we note that the scanning curve and the maximum field distribution on the scanning curve in the case of CSE definition depend on the parameters F and U in the same way as in the case considered above. So we present only one Figure 11 a, b, which show dependencies $z_s(y_s)$ (Fig. 11 a) and $K_m(y_s)$ (Fig. 11 b), where K_m is the CSE maximum value. Curves 1 – 3, as before, correspond to three types of arrays. They are obtained for $F = 1000$, $U = 2$, $X_m = Y_m = 300$, $f_0 = 10$ ГГц, $\Delta = 0$.

It can be seen that the scanning curves pass through the predicted focal point and they all intersect in this point. The reasons for the appearance of the intersection point were explained above. Similarly curves 1 – 3 in Fig. 11 b also have a common point of intersection, in which the CSE in dB is close to zero. However, it must not be equal to exactly zero at any point, since the amplitude distribution of the sources in the aperture differs from the optimal one.

In conclusion of this section we will consider the behavior of an array operating on the zero space harmonic. As noted above, arrays of this type take a special place among arrays with the frequency scanning, since they can focus the field only at a point located outside of the array aperture: $y_f > Y_m$. This increases the real focal distance that is equal to the distance from the array center to the focal point. It is equal to $\sqrt{F^2 + y_f^2}$. Also an important feature of the array is the influence of its geometric parameters on its operating frequency range. This is due to the necessity of fulfilling the condition (8).

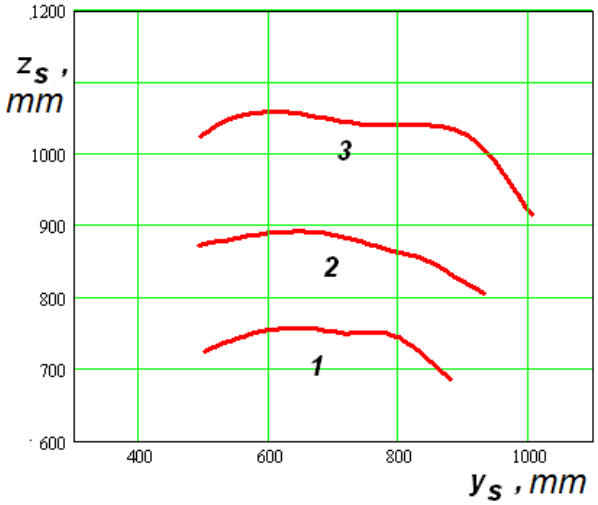

Fig. 12. Scanning curves. Zero order harmonic. Maximum intensity definition.

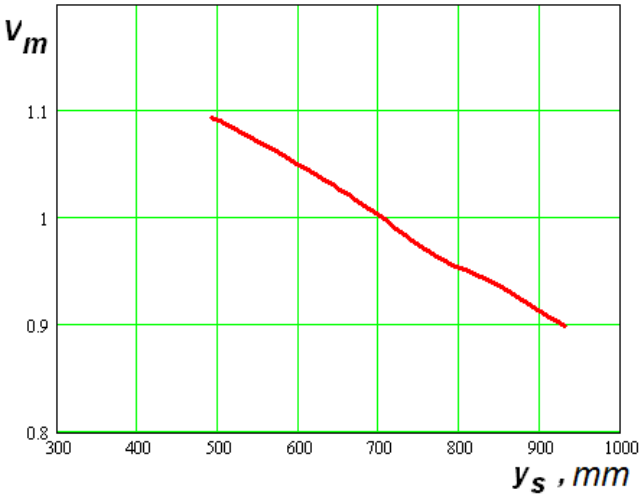

Fig. 13. Maximum intensity distribution. Zero order harmonic. Maximum intensity definition.

The scanning curves of an array with zero order harmonic are shown in Fig. 12. Curves 1 – 3 are obtained for F=800, 1000, 1200, y_f=700, $f_0 = 10$ ГГц, $X_m = Y_m = 300$. The array scans in the 3 GHz band. In this case curves 1 – 3 correspond to the lower frequencies of the operating range 9.16, 9.44, 9.62 GHz. The change in the lower frequency is due to the change of parameter F, which affects the waveguide dimensions in the synthesis of the array.

It can be seen from Fig. 12 that the focal spot moves mainly in the horizontal plane. The coordinate z changes slightly. In some parts of the scanning curve this change is very small. This result looks unexpected, since in the examples presented

above the focal spot moves predominantly perpendicular to radius-vector connecting the array center to the focal point. It is seen from Fig. 12 that in the considered case this condition is not satisfied and the focal spot moves in another direction.

The length of the scanning curve is relatively small, if compared with the curves for arrays with minus first harmonic and also to take into account the relatively large focal distance. That is, in terms of the width of the frequency scanning sector relative to the frequency range this type of arrays is worse comparing with those considered above. However its advantage is a relatively small change in the maximum value of the intensity when scanning.

The dependence of the normalized maximum intensity of the field V_m on the coordinate y_s is shown in Fig. 13. The normalization as before is carried out on the value of the intensity at the synthesis frequency f_0. From Fig. 13 it follows that the aberrations that reduce the value of V_m are relatively small and its changes are likely due to an increase in the distance from the array to the point of focusing.

The scan parameters obtained with help of CSE are shown in Fig. 14 and 15. The scanning curve is presented in Fig. 14 and the maximum CSE distribution on it is given in Fig. 15. As was expected, the scanning curve determined with the aid of CSE passes through the calculated focal point.

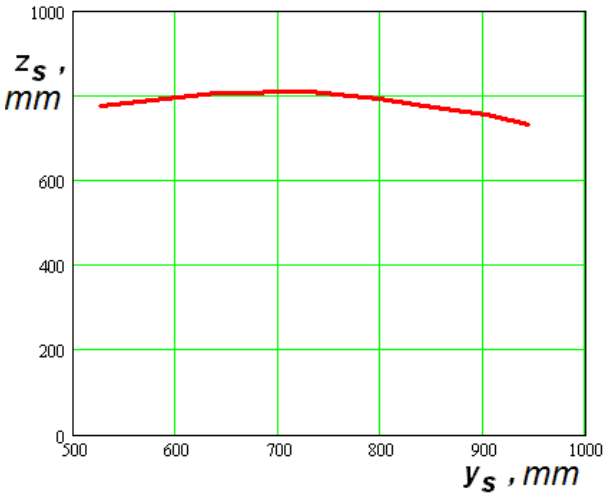

Fig. 14. Scanning curves. Zero order harmonic. Maximum CSE definition.

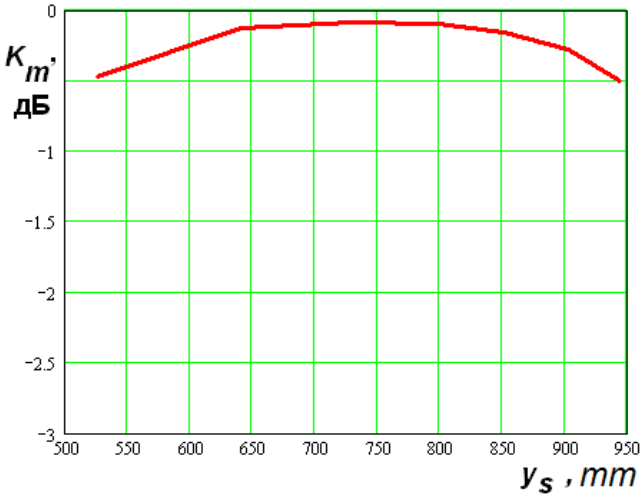

Fig. 15. Maximum CSE distribution. Zero order harmonic. Maximum CSE definition.

Note that it is closer to the horizontal line than the curves shown in Fig. 12. The CSE on the scanning curve has small variations not greater than 0.5 dB (see Fig. 15).

5. Numerical study of focused arrays scanning in the main transverse plane

Let us consider the behavior of focused arrays in the main transverse plane of scanning, that is, in the *XOZ* plane. We will only analyze arrays that operate at minus first harmonic. Scanning in this plane is performed at the single frequency f_0, on which all arrays are equivalent to each other. It facilitates their analysis, since it is sufficient to consider only one of them. Take for example an array with a constant period and a phase shifters system.

Scanning in the transverse plane occurs due to the change in the parameters of the AEC. As noted above, the AEC performs the function of a lens located at $y = -Y_m$ and focusing the field at the point $(0,0,F)$. Consider the scan, which the AEC performs, focusing the field to the point $(x_f,0,F)$. In so doing, we suppose that the AEC has no aberrations. This assumption makes it possible to investigate the errors caused solely by the array itself.

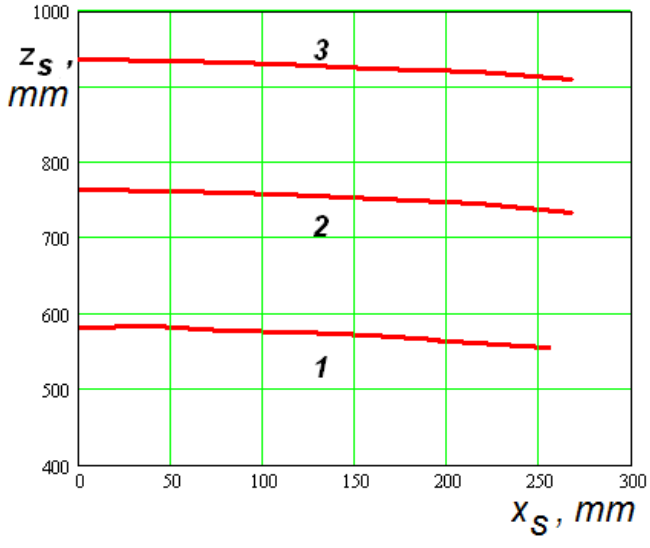

Fig. 16. Scanning curves in transversal plane. Maximum intensity definition. *F*=600,800,1000.

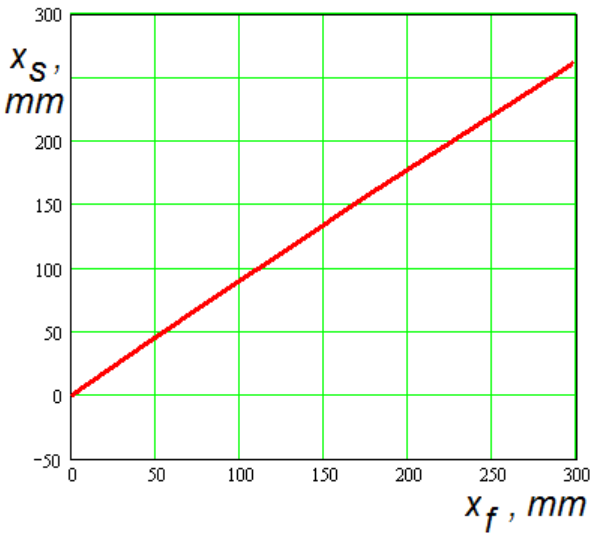

Fig. 17. Dependence of coordinate x_s versus coordinate x_f.

The scanning curves obtained by the criterion of field maximum are shown in

Fig. 16. Curves 1 - 3 are calculated for $F = 600,800,1000$, $f_0 = 10$ ГГц, $X_m = Y_m = 300$, $U = 2$. The coordinate of the focal point x_f changes in the range from zero to 300. The coordinate of the point of field maximum x_s is uniquely related to x_f.

The dependence $x_s(x_f)$ is presented in Fig. 17. It is described with good accuracy by a linear function. However, the angle of its tilt is a slightly less than 45^0. Therefore, the scanning sector determined by x_s is less than the range of the parameter x_f change. Curves 1 - 3 in Fig. 16 lie below the corresponding values of the focal distance F, like it was in all the cases considered above.

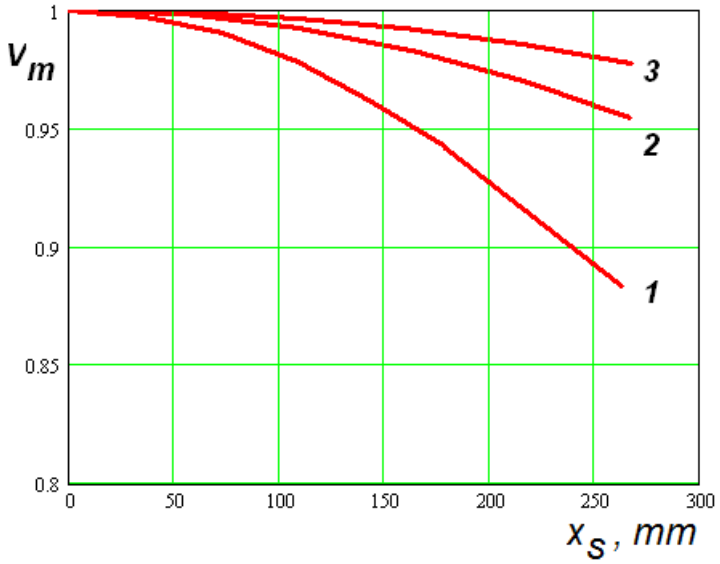

Fig. 18. Maximum field intensity distribution on the scanning curve.
F=600,800,1000.

The most interesting is the dependence of the normalized maximum field intensity on variable x_s shown in Fig. 18. The field intensity is normalized on its value at the point $x_s = 0$. Curves 1 – 3 are obtained for the parameters given above. We can see that the movement of the focal point almost to the array edge ($X_m = 300$) has very little effect on the maximum field intensity V_m. This influence becomes more noticeable in short-focus structures ($F = 600$). In relatively long-focus arrays, it is very small even at large displacements x_s of the focal point.

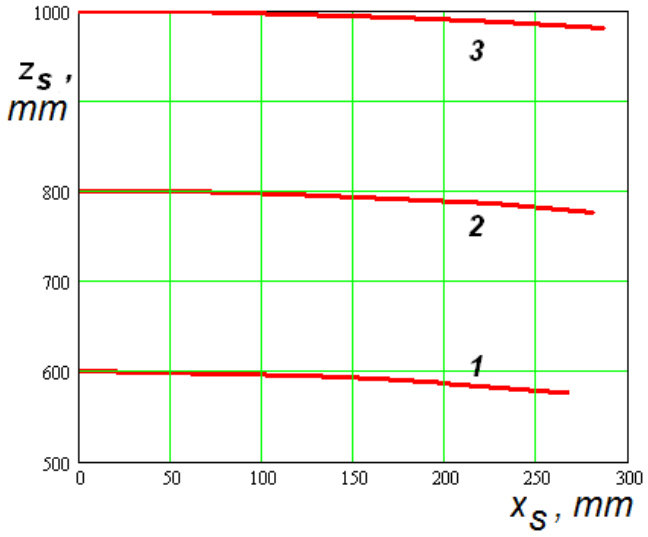

Fig. 19. Scanning curves in transversal plane. Maximum CSE definition. F=600,800,1000.

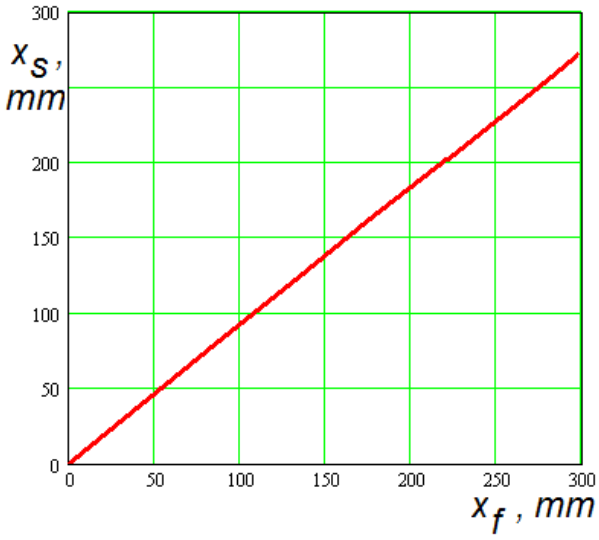

Fig. 20. Dependence of coordinate x_s versus coordinate x_f.

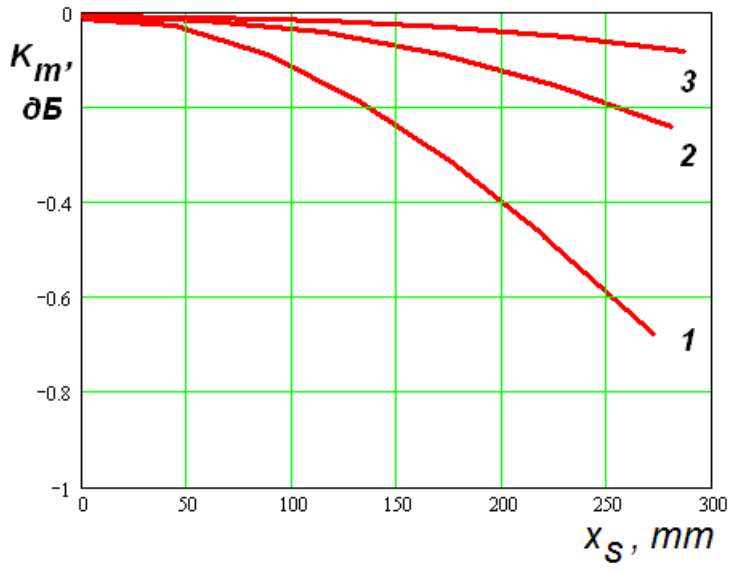

Fig. 21. Maximum CSE distribution along scanning curve. F=600,800,1000.

The array demonstrates the similar behavior if the maximum CSE is taken as a criterion. The corresponding scanning curves are presented in Fig. 19. Curves 1 – 3 are calculated for the array parameters given above. It is seen that they pass through the point $(0,0,F)$. As the parameter x_s is increased, the distance from the array plane to the focusing point is slightly decreased. The dependence $x_s(x_f)$ found using the CSE is shown in Fig. 20. It is close to linear.

The dependence of the maximum CSE on the coordinate x_s obtained for the above parameters is presented in Fig. 21. There is a slight drop in the CSE on the scanning curve. Except for the case $F = 600$, it does not exceed 0.25 dB.

Thus from the results of the scanning study in the main transverse plane it follows that the focused planar arrays have good optical properties in the main transverse plane, since in with an ideal AEC the scanning does not lead to a strong decrease in the field intensity and a large decrease in the CSE.

Conclusion

The results of investigation of different types of arrays presented in this paper allow us to draw the following conclusions:

1. The asymmetry of the scanning curve found in [24], [25] is not a consequence of the operating principles of arrays with frequency scanning. It is caused by a specific type of TL and the array structure.
2. Single-focus arrays with a constant period operating at minus first harmonic in many respects are superior over those with a constant slowing factor.
3. The aberrations in the main transverse plane of scanning are relatively small. In particular they are noticeably smaller than the aberrations in the longitudinal plane of scanning.
4. The array at the zero-order radiating space harmonic is inferior to the arrays at the minus first harmonic, but it is of interest due to the special shape and location of the scanning curve.

References

1. David M. Sheen, Justin L. Fernandes, Jonathan R. Tedeschi, Douglas L. McMakin, A. Mark Jones,Wayne M. Lechelt, and Ronald H. Severtsen, Wide-bandwidth, wide-beamwidth, high-resolution, millimeter-wave imaging for concealed weapon detection, *Proc. of SPIE,* Vol. 8715 871509-1.
2. D.A. Robertson, S.L. Cassidy, B. Jones, A. Clark, in Passive and Active Millimeter-Wave Imaging XVII, Proc. of SPIE, vol. 9078, ed. by D.A. Wikner,

A.R. Luukanen (2014), *Proc. of SPIE*, vol. 9078, p. 907805. doi:10.1117/12. 2053023.

3. S.S. Ahmed, A. Schiessl, L.-P. Schmidt, et al., A novel fully electronic active real-time imager based on a planar multistatic sparse array, *IEEE Transactions on Microwave Theory and Techniques*, 2011, 59, p. 3567-3576.
4. N. J. Bowring, M. J. Southgate, D. A. Andrews, et al., Development of a longer range standoff millimeter wave radar concealed threat detector. *Proc. of SPIE*, Vol. 8714 87140C.
5. E. Heinz, T. May, D. Born, G.l. Zieger, et al., Toward high-sensitivity and high-resolution submillimeter-wave video imaging *Opt. Eng*., 50(11), November 02, 2011.
6. E. N. Grossman, J. Gordon, D. Novotny, R. Chamberlin, Terahertz active and passive imaging, 2014 8th European Conference on Antennas and Propagation (EuCAP), DOI: 10.1109/EuCAP.2014.6902253.
7. N.E. Alexander, B. Alderman, F. Allona, et al, TeraSCREEN: multi-frequency multi-mode Terahertz screening for border checks. *Proc. of SPIE,* Vol. 9078 907802-1.
8. E. Gandini, N. Llombart, A. Neto, T. Bryllert, E.Gandini, N.Llombart, Near-field imaging system fed by lens antenna focal plane array at sub-millimeter frequency. Proc. of IEEE Europ. Conf. on Antennas and Propagation, Apr.6-11, Hague, Netherland, 2014.
9. Sheen, D.M., McMakin D.L., and Hall T.E., Combined illumination cylindrical millimeter-wave imaging technique for concealed weapon detection. *Proc. of SPIE*, 2000. 4032: p. 52-60.
10. Sheen, D.M., D.L. McMakin, and T.E. Hall, Cylindrical millimeter-wave imaging technique for concealed weapon detection. Proceedings of SPIE, 1997. 3240: p. 242-250.
11. E. Schreiber, M. Peichl, M. Jirousek, H. Suess. VESAS: a novel concept for fully-electronic passive MW imaging. *Proceedings of SPIE Defense, Security, and*

Sensing. 2013, 8715 (87150J). SPIE Digital Library. SPIE Defense, Security, and Sensing 2013, Apr 29 –May 3, 2013, Baltimore, USA.

12. I. Ohtera, Focusing properties of a microwave radiator utilizing a slotted rectangular waveguide. *IEEE Trans. on Antennas and Propagation*, 1990, V. 38, N. 1, p. 121-124.
13. I. Ohtera, Diverging/focusing of electromagnetic waves by utilizing the curved leakywave structure: Application to broad-beam antenna for radiating within specified wide-angle. *IEEE Trans. on Antennas and Propagation*, 1999, V. 47, N. 9, p.1470-1475.
14. J. L. Gómez-Tornero, F. Quesada-Pereira, A. Alvarez-Melcón, et al., Frequency steerable two dimensional focusing using rectilinear leaky-wave lenses, *IEEE Trans. on Antennas and Propagation*, V. 59, N. 2, 2011, p. 407-415.
15. A. J. Martínez-Ros, J. L. Gómez-Tornero, F. J. Clemente-Fernández, J. Monzó-Cabrera, Microwave near-field focusing properties of width-tapered microstrip leaky-wave antenna. *IEEE Trans. on Antennas and Propagation*, VOL. 61, N. 6, 2013, p. 2981-2990.
16. T. Okuyama, Y. Monnai, H. Shinoda, 20-GHz focusing antennas based on corrugated waveguide scattering. *IEEE Antennas and Wireless Propagation Letters*, V. 12, 2013, p. 1284-1286.
17. S. Clauzier, S. Avrillon, L. Le Coq, M. Himdi, F. Colombel, E. Rochefort, Slotted waveguide antenna with a near-field focused beam in one plane. *Microwaves, Antennas & Propagation*, IET, 2014, Volume: 9, Issue: 7, p. 634- 639, https://hal.archives-ouvertes.fr/hal-01114680/document.
18. M. L. Chen , S. Gupta, Z. L. Ma, L. J. Jiang, Linearly Polarized Near Field Focused Slot-Array Waveguide, Antennas and Propagation Society International Symposium (APSURSI), IEEE, 6-11 July , 2014, p. 1047–1048, Memphis, USA.
19. J. L. Gómez-Tornero, A. J. Martinez-Ros , N. D.Blanco, E. Rajo-Iglesias, Near-field focusing with holographic two-dimensional tapered leaky-wave slot antennas. Proc. of the 6th European Conf. on Antennas and Propagation (EUCAP), 2012, p. 234-238.

20. D. Blanco, J.L. Gómez-Tornero, E. Rajo-Iglesias, N. Llombart, Radially polarized annular-slot leaky-wave antenna for three-dimensional near-field microwave focusing. *IEEE Antennas and Wireless Propagating Letters*, V. 13, 2014, p. 583-586.

21. M. Ettorre, M. Casaletti, G.Valerio, R. Sauleau, L. Le Coq, S. C. Pavone, M. Albani, On the near-field shaping and focusing capability of a radial line slot array. *IEEE Trans. on Antennas and Propagation*, V. 62, N. 4, April 2014, p. 1991-1999.

22. S. E. Bankov, V. A. Kaloshin, and E. V. Frolova, Synthesis and Analysis of a Frequency_Scanned Planar Waveguide Array Focused in the Fresnel Zone. *Journal of Communications Technology and Electronics*, 2016, Vol. 61, No. 6, pp. 587–597.

23. S. E. Bankov and E. V. Frolova, Synthesis and Analysis of a Planar Waveguide Array with Two-Dimensional Frequency Scanning Focused in the Fresnel Zone. *Journal of Communications Technology and Electronics*, 2017, Vol. 62, No. 9, pp. 927–940.

24. T.A. Milligan, Modern antenna design. USA, New Jersey, JOHN WILEY & SONS, INC., 2005.

25. Rotman W. and Turner R.F. Wide-Angle Microwave Lens for Line Source Applications. // IEEE Transactions on AP. 1963. V. 11. N. 11. P. 623-632.

For citation:
Sergey E. Bankov. 2D single–focus frequency scanning arrays focused in the Fesnel zone. *Zhurnal Radioelektroniki - Journal of Radio Electronics*. 2017. No. 10. Available at http://jre.cplire.ru/jre/oct17/13/text.pdf.